Journal of the European Ceramic Society 5 (1989) 245–256

The Microstructure and Composition of Oxide Films Formed during High Temperature Oxidation of a Sintered Silicon Nitride

P. Andrews & F. L. Riley

Division of Ceramics, School of Materials, The University of Leeds, Leeds LS2 9JT, UK

(Received 7 August 1989; accepted 4 October 1989)

Abstract

The oxidation behaviour of a sintered silicon nitride has been studied in the temperature range 1300°C to 1400°C. The oxide film appears to give some protection to the silicon nitride, but above a critical temperature (~1385°C) greatly increased rates of oxidation are observed. This behaviour, and microstructural and compositional changes seen in the oxide film, are explained in terms of experimentally determined phase relationships in the $MgSiO_3$–SiO_2–$Y_2Si_2O_7$ system. A model is proposed for the oxidation process emphasising the possible importance of a thin protective layer of cristobalite at the nitride/oxide film interface.

Das Oxidationsverhalten eines gesinterten Siliziumnitrids wurde im Temperaturbereich von 1300°C bis 1400°C untersucht. Die Oxidschicht scheint das Siliziumnitrid etwas zu schützen, oberhalb einer kritischen Temperatur (~1385°C) aber steigt die Oxidationsrate stark an. Dieses Verhalten, die Änderungen der Mikrostruktur und die Änderungen der Zusammensetzung im Oxidfilm werden durch experimentell bestimmte Phasenbeziehungen im System $MgSiO_3$–SiO_2–$Y_2Si_2O_7$ erklärt. Es wird ein Modell für den Oxidationsprozeß vorgeschlagen, das den möglicherweise positiven Effect einer dünnen, schützenden Schicht aus Cristobalit an der Nitrid-Oxidschicht-Grenzfläche hervorhebt.

Le comportement à l'oxydation d'un nitrure de silicium fritté a été étudié à des températures allant de 1300 à 1400°C. La couche d'oxyde semble protéger le nitrure de silicium, mais les vitesses d'oxydation augmentent fortement au-delà d'une température critique (~1385°C). Ce comportement et des changements de la microstructure et de la composition observés dans la couche d'oxyde sont expliqués par des relations de phases déterminées expérimentalement dans le système $MgSiO_3$–SiO_2–$Y_2Si_2O_7$. On propose un modèle du processus d'oxydation faisant ressortir l'importance possible d'une fine couche protectrice de cristobalite à l'interface nitrure/couche d'oxyde.

1 Introduction

Because of their high temperature properties sintered silicon nitride ceramics are being developed for structural components in gas turbine engines with projected material surface temperatures of ~1400°C. This represents a significant increase in operating temperature compared with the current metal superalloys and is expected to lead to improvements in engine efficiency. The gas turbine environment is strongly oxidising. An understanding of the mechanisms of oxidation of sintered silicon nitride materials is therefore important, not least because it will guide the selection of sintering additive systems. Metal oxides are normally used to ensure attainment of full density of the silicon nitride through liquid phase sintering. On cooling from the sintering temperature the liquid solidifies to form secondary phases, saturated with nitrogen,[1] in the silicon nitride intergranular regions. These phases can be amorphous and/or crystalline, depending on the system, the starting composition within that system and the heat treatment. The secondary phases are believed to be responsible for the generally faster oxidation rates of sintered (or hot pressed) silicon nitrides, compared with those of pure, single phase, silicon nitride.[2]

It is generally accepted that a major rate controlling process in the oxidation of sintered silicon nitride involves the outward diffusion of

Journal of the European Ceramic Society 0955-2219/90/S3.50

cations and/or anions from the secondary phase material, rather than the inward diffusion of oxygen through a growing protective oxide film.[3] This view is based on observations that oxidation rates are apparently independent of the oxide film thickness.[4,5] The outward diffusion of cations (with charge balancing anions) occurs due to the chemical potential gradients between the metal oxide-rich secondary phase and the initially pure silicon dioxide forming at the silicon nitride/gas interface by oxidation of silicon nitride grains. The product oxide film is usually partially crystalline,[6] and may contain cristobalite, together with crystalline silicates formed by reaction of secondary phase metal oxides[7,8] with the silicon dioxide primary oxidation product. Qualitative and semi-quantitative X-ray diffraction (XRD) examinations of oxide films have been reported for silicon nitride materials densified with magnesium oxide (MgO),[4,7-9] yttrium oxide (Y_2O_3),[10] cerium oxide (CeO_2)[11] and MgO with Y_2O_3.[12]

We report here investigations of the nature of the oxide films formed by the high temperature oxidation of a sintered silicon nitride densified with Cr_2O_3, MgO and Y_2O_3. A supporting study of phase equilibrium relationships in the SiO_2-rich corner of the $MgO–SiO_2–Y_2O_3$ phase diagram was carried out to provide information about the oxidation product system. Phases formed in the oxide film are explicable in terms of the phase relationships in the $MgSiO_3–SiO_2–Y_2Si_2O_7$ compatibility triangle of this system.

Although three oxides, Cr_2O_3, MgO and Y_2O_3, were used as densification additives for the silicon nitride studied in this programme, observations of the product oxide film and bulk unoxidised material using scanning electron microscopy (SEM), XRD and electron probe micro-analysis (EPMA) indicated that phase relationships in the material could be satisfactorily treated in terms of the simpler $MgO–SiO_2–Y_2O_3$ ternary system.

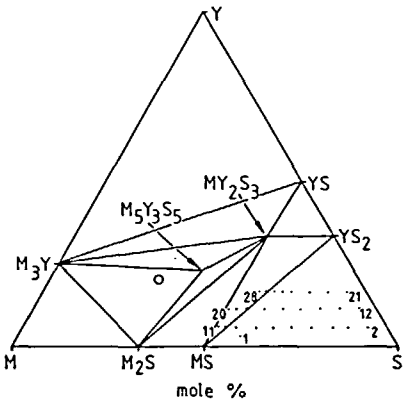

Fig. 1. The Mg–Si–Y–O phase diagram (after Ref. 13). Points 1–28 represent the compositions examined in the present work. O, Calculated composition of the intergranular phase of the silicon nitride.

M—MgO MS—$MgSiO_3$ M_2S—Mg_2SiO_4
MY_2S_3—$MgY_4Si_3O_{13}$ M_3Y—$Mg_3Y_2O_6$ $M_5Y_3S_5$—$Mg_5Y_6Si_5O_{24}$
S—SiO_2 Y—Y_2O_3 YS—Y_2SiO_5
YS_2—$Y_2Si_2O_7$

2 Experimental

2.1 Phase relations in the $MgO–SiO_2–Y_2O_3$ system

Compositions mainly within the $MgSiO_3–SiO_2–Y_2Si_2O_7$ triangle (Fig. 1 and Table 1) were examined at 1300°C and 1400°C. They were prepared from appropriate amounts of MgO, SiO_2 and Y_2O_3 powders, details of which are given in Table 2.

Table 1. Compositions examined in the phase diagram study

Number	*Mole%*		
	MgO	*SiO_2*	*Y_2O_3*
1	39·0	58·0	3·0
2	5·0	89·5	5·5
3	10·0	84·5	5·5
4	14·0	80·5	5·5
5	19·5	75·0	5·5
6	24·5	70·0	5·5
7	29·5	65·0	5·5
8	34·0	60·5	5·5
9	39·0	55·5	5·5
10	41·5	53·0	5·5
11	44·0	50·5	5·5
12	4·5	84·5	11·0
13	9·5	79·5	11·0
14	14·5	74·5	11·0
15	19·5	69·5	11·0
16	24·0	65·0	11·0
17	29·0	60·0	11·0
18	34·0	55·0	11·0
19	36·5	52·5	11·0
20	38·5	50·5	11·0
21	5·0	79·0	16·0
22	10·0	74·0	16·0
23	14·5	69·5	16·0
24	19·5	64·5	16·0
25	21·5	62·5	16·0
26	24·0	60·0	16·0
27	26·5	57·5	16·0
28	29·0	55·0	16·0

Table 2. Details of powders used in the phase diagram study

	Suppliers	*Purity (%)*	*Loss on drying (mass%)*
SiO_2	BDH Chemicals	Precipitated acid washed	8
MgO	May and Baker	>96·0	9
Y_2O_3	Aldrich	99·99	1

Loss on drying determined by TGA. Powders heated to 650°C.

The powders were mixed by mechanical shaking in propan-2-ol for 1 ks, followed by drying under an infra-red lamp with mechanical stirring. The mixtures were then pressed into ~0·6 g pellets of 15 mm diameter and heated in covered platinum crucibles in a muffle furnace. The equilibration heating schedule was:

(1) 1550°C for 11 ks;
(2) cool to required temperature (1400°C or 1300°C) and hold for 54 ks;
(3) water quench.

XRD and EPMA were used to identify crystalline phases and to confirm phase compositions.

The ternary eutectic temperature in the $MgSiO_3$–SiO_2–$Y_2Si_2O_7$ compatibility triangle was subsequently determined using a hot-stage microscope to observe the onset of liquid formation in a pre-equilibrated mixture corresponding to the estimated eutectic composition.

2.2 Silicon nitride oxidation

A sintered reaction bonded silicon nitride (SRBSN) designated '10.2.2' by the suppliers (British Ceramic Research Laboratories, Stoke-on-Trent, UK) was used. This designation refers to the approximate sintering additive composition in mass% (Table 3). The three oxides had been mixed with silicon powder, which had then been compacted, nitrided and finally sintered to full density using the standard powder bed method. Further details of the material are given in European patent application 0 107 919.[13]

The silicon nitride was supplied as a tile ~150 mm × 150 mm × 12 mm. A minimum of 1·5 mm was ground from all surfaces to remove a layer of material which showed significant structural differences compared with the interior. Characterisation of the bulk material entailed chemical analysis by EPMA and by atomic absorption spectroscopy (AAS), microstructural examination by SEM, density measurements by mercury immersion and crystalline phase content determination by XRD analysis of ground material.

Samples were prepared for AAS by crushing the silicon nitride in a tungsten carbide percussion mill to pass through a 53 μm sieve. Approximately 0·1 g of powder was accurately weighed and heated to fusion in a platinum crucible with a known quantity (~0·5 g) of K_2CO_3. The fused mass was quenched and dissolved in ~50 ml of 10% HCl to provide a solution for AAS analysis.

Samples, ~4 mm × 4 mm × 8 mm, were cut from the tile and prepared for oxidation by grinding with 400-mesh silicon carbide powder, followed by ultrasonic cleaning under acetone. Oxidation was studied at temperatures between 1300°C and 1400°C for times up to ~430 ks (~120 h) in an atmosphere of flowing laboratory air (1·5 $cm^3 s^{-1}$). Individual samples were oxidised for set periods in a vertical tube furnace, after which mass changes were determined by weighing to ±10 μg. Data were normalised to mass gain per unit area of surface (Δ). The surfaces of oxidised samples were examined by XRD. SEM and EPMA were used to examine the microstructure and composition of polished sections of oxidised material.

Table 3. Composition of silicon nitride

	Designated composition		*Chemical analysis*			
			EPMA		*AAS*	
	Mass%	*Mole%*	*Mass%*	*Mole%*	*Mass%*	*Mole%*
Y_2O_3	10	6·15	8·9	5·1	9·2	5·4
MgO	2	6·89	4·5	14·6	4·3	14·0
Cr_2O_3	2	1·83	2·1	1·8	2·5	2·2
Si_3N_4	bal.	bal.	bal.	bal.	bal.	bal.

Cations determined by EPMA and AAS, and expressed as notional oxide content.

3 Results

3.1 Phase relations in the MgO–SiO_2–Y_2O_3 system

The phase fields formed in the SiO_2–$MgSiO_3$–$Y_2Si_2O_7$ compatibility triangle after equilibration at 1400°C are shown in Fig. 2. The phase fields were identified from XRD analyses of samples of known composition, and showed that a liquid region was formed close to the $MgSiO_3$–$Y_2Si_2O_7$ join. The

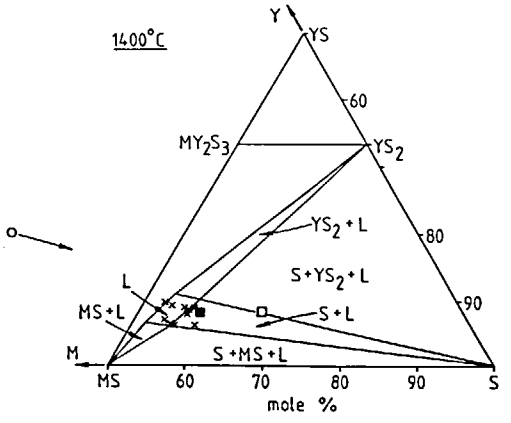

Fig. 2. Section of the SiO_2-rich corner of the MgO–SiO_2–Y_2O_3 phase diagram at 1400°C. Symbols as defined in Fig. 1. ×, EPMA compositions of glasses formed during equilibration; ■, EPMA composition of glass formed in outer oxide scale at 1400°C; L, liquid; □, EPMA composition of glass formed at nitride/oxide interface at 1400°C.

presence of liquid was deduced from the absence of an Mg-, Si- or Y-containing crystalline phase. Compositions of liquids formed in the samples at 1400°C, as determined by EPMA, are also shown. These analyses showed satisfactory agreement with the liquid region established by XRD. A pre-equilibrated composition at the estimated centre of the liquid phase region (MgO 37·5 mole%, SiO_2 54·5 mole% and Y_2O_3 8·0 mole%) had a maximum melting temperature of 1385°C from repeated observations made using a hot-stage microscope.

Equilibration at 1300°C gave by XRD analysis, as expected, proto-enstatite ($MgSiO_3$), cristobalite (SiO_2) and yttrium disilicate ($Y_2Si_2O_7$) in all compositions within the $MgSiO_3$–SiO_2–$Y_2Si_2O_7$ compatibility triangle.

3.2 Silicon nitride starting material

The composition of the silicon nitride, as determined by EPMA and AAS, is shown in terms of notional oxide content in Table 3. Microstructural observations (Fig. 3) showed that the Cr_2O_3 had lost oxygen during sintering to form chromium disilicide, $CrSi_2$, as localised inclusions in the intergranular silicate phase:

$$2Cr_2O_3 + Si_3N_4 \rightarrow 4Cr + 3SiO_2 + 2N_2$$
$$\Delta G^\circ_{1700\,K} = -260\,kJ\,mol^{-1} \quad (1)$$
$$Cr + 2Si \rightarrow CrSi_2$$
$$\Delta G^\circ_{1700\,K} = -80\,kJ\,mol^{-1} \quad (2)$$

On the assumption that the oxygen from the Cr_2O_3 combines with the silicon of the Si_3N_4 to form SiO_2, and that ~2% SiO_2 (by mass) was initially present in the Si_3N_4 starting powder, full equilibration in the MgO–SiO_2–Y_2O_3 system during sintering gives an overall secondary phase composition of MgO 52 mole%, SiO_2 28 mole% and Y_2O_3 20 mole% (Figs 1 and 2).

XRD analysis of a powdered sample of silicon nitride showed β-Si_3N_4 as the major crystalline phase; other peaks were very weak and could not be indexed with any degree of certainty. The density of the bulk material was 3·21 $Mg\,m^{-3}$.

3.3 Low temperature oxidation

At temperatures between 1300°C and 1385°C measurements of mass gain per unit area (Δ) showed that oxidation closely followed parabolic kinetics over times up to 300 ks (~85 h) (Fig. 4). Parabolic rate constants were determined from the slopes of plots of Δ^2 as a function of time.

XRD analysis of the surfaces of samples oxidised at temperatures up to 1385°C showed the presence of α-cristobalite (SiO_2), proto-enstatite ($MgSiO_3$) and yttrium disilicate ($Y_2Si_2O_7$). The underlying β-Si_3N_4 was the only other phase detected, the peaks of which became weaker with increasing time of oxidation. By applying a semi-empirical correction factor to the measured XRD peak heights, an assessment of the amounts of the phases present in the oxide film was possible. The correction factor was derived by comparing the mean reduction in intensity of the β-Si_3N_4 peaks in the oxidised samples with the corresponding peaks in the unoxidised material. Peak height measurements (I) of the phases were taken as the summation of the strongest diffracting planes: (101) for SiO_2; (220), (310) and (102) for $MgSiO_3$; (12$\bar{1}$), (111) and (210) for $Y_2Si_2O_7$; and (101), (210) and (200) for β-Si_3N_4. Plots of the square of the corrected peak height intensity (I^2) as a function of time at 1300°C, 1350°C and 1385°C are shown in Figs 5, 6 and 7 respectively. Arrhenius treatment (Fig. 8) applied to the linear regions of these graphs suggested that the amounts present both of cristobalite and of proto-enstatite followed a smooth relationship, whereas the forma-

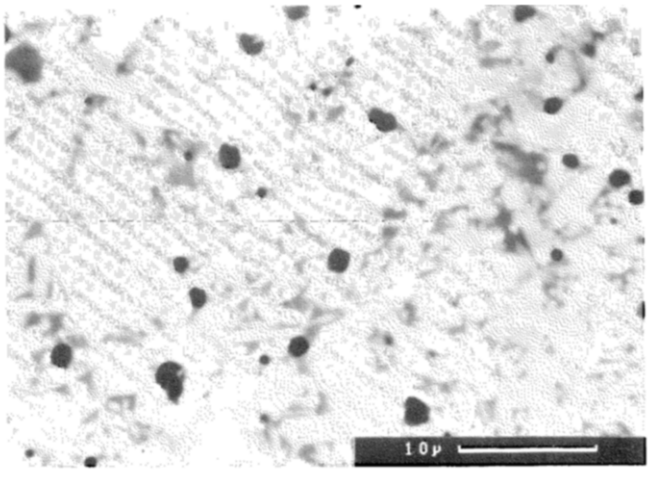

Fig. 3. Back-scattered electron micrograph of silicon nitride microstructure. Dark particles, $CrSi_2$ inclusions; light coloured acicular grains, silicon nitride; intermediate grey, intergranular secondary phase.

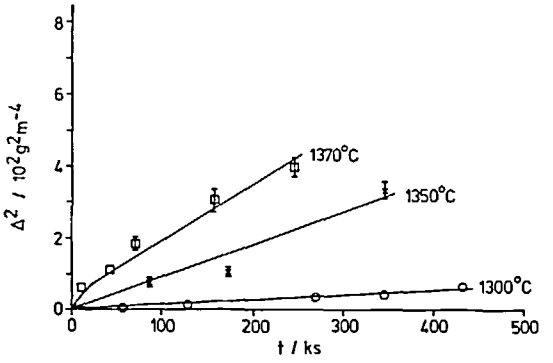

Fig. 4. Mass gain per unit area squared, Δ^2, as a function of time at 1300°C, 1350°C and 1370°C.

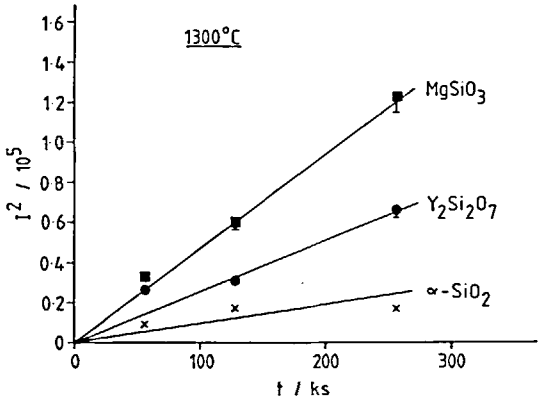

Fig. 5. XRD peak height intensity squared, I^2, as a function of time at 1300°C.

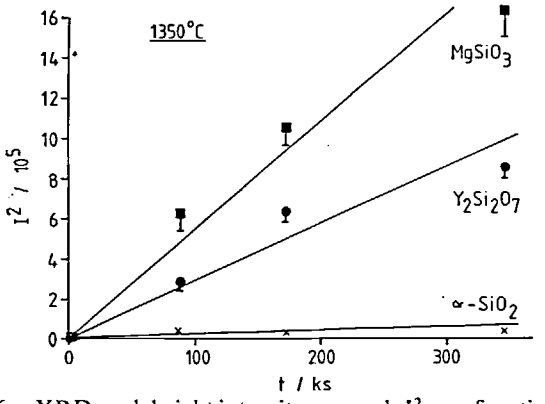

Fig. 6. XRD peak height intensity squared, I^2, as a function of time at 1350°C.

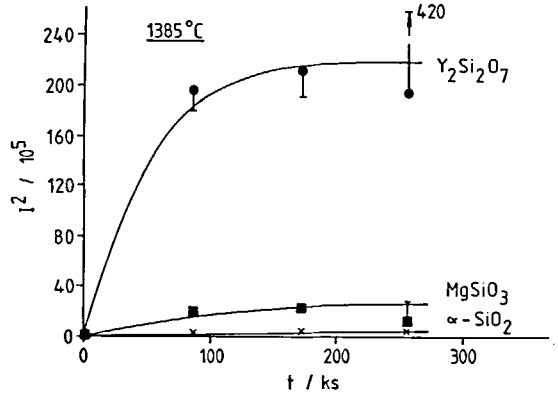

Fig. 7. XRD peak height intensity squared, I^2, as a function of time at 1385°C.

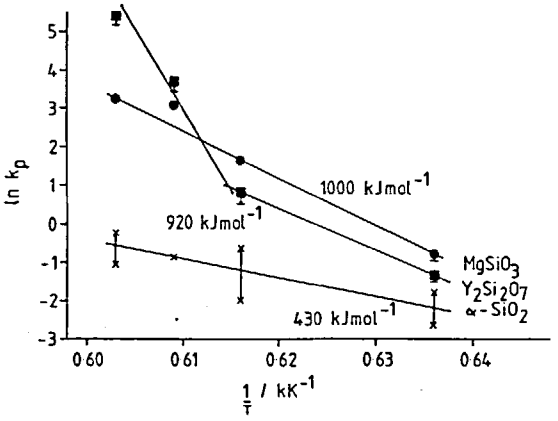

Fig. 8. Arrhenius treatment of XRD peak height data.

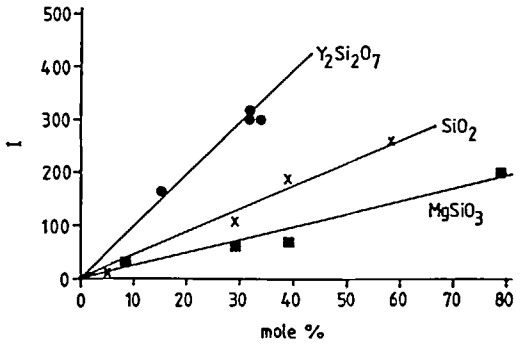

Fig. 9. Relative XRD peak heights of α-cristobalite, proto-enstatite and yttrium disilicate for equivalent molar percentages.

tion of yttrium disilicate became markedly more pronounced above ~1350°C.

XRD peak intensities for mixtures of known proportions of the three phases were recorded under identical conditions to provide the basis for assessment of the compositions of the oxide films. Because it proved difficult to prepare pure proto-enstatite, the samples obtained earlier from the construction of the phase equilibrium diagram at 1300°C were used. These samples had been quenched from 1300°C to room temperature, and were finely crushed for XRD examination. For each component a plot of the summed peak height I as a function of proportion present in the mixture of the three gave a smooth curve (Fig. 9). The slopes of these lines were later used to estimate the molar proportions of each crystalline component in the oxide film.

Microstructural and EPMA examination of the oxide films formed at temperatures below 1385°C showed (Fig. 10) a layered structure in which cristobalite was mainly present as a thin film at the nitride/oxide interface, and proto-enstatite in a thicker layer outside the cristobalite. The yttrium disilicate was predominantly present as separate crystals at or close to the silicate/air interface. Large

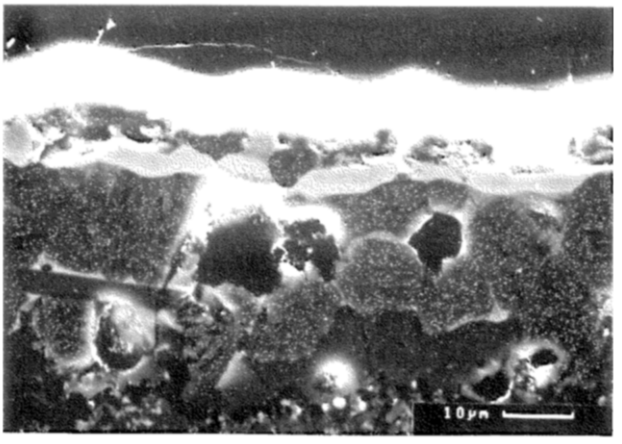

Fig. 10. Silicon nitride oxidised at 1370°C for ~85 ks. Secondary electron image shows bright $Y_2Si_2O_7$ inclusions in an $MgSiO_3$ matrix and a layer of SiO_2 at the oxide/nitride interface. The superimposed X-ray dot map is for Mg.

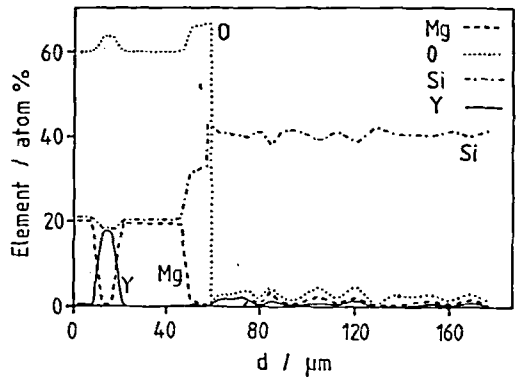

Fig. 11. EPMA line scan of material oxidised at 1370°C for 85 ks.

irregularly shaped voids were present in the outer regions of the oxide film, and the nitride/oxide interface was clearly delineated by the presence of small pores. The total pore volume increased with oxidation time and temperature.

EPMA was used to confirm the distribution of phases in the oxide film, and to follow the diffusion of cations from the silicon nitride to the oxide. A typical line scan of material oxidised at 1370°C for 85 ks is shown in Fig. 11. This indicates clearly the concentration of $Y_2Si_2O_7$ near the oxide–air interface, and a marked depletion of intergranular Mg^{2+} just inside the unoxidised silicon nitride.

The third major additive ion, Cr^{3+}, was detected only at very low levels, at the nitride–oxide interface. Significant migration of Cr^{3+} from the silicon nitride did not occur. Most of, if not all, the chromium in the silicon nitride exists as small $CrSi_2$ inclusions. The small amount of Cr detected by EPMA in the surface oxide film tended also to be localised in discrete regions near the silicon nitride–oxide interface, rather than homogeneously distributed.

3.4 High temperature oxidation

At 1400°C oxidation rates were significantly faster than might have been expected from an extrapolation of lower temperature data. Kinetics were

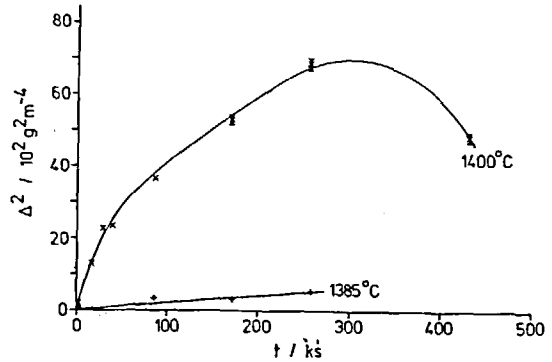

Fig. 12. Mass gain per unit area squared, Δ^2, as a function of time at 1385°C and 1400°C.

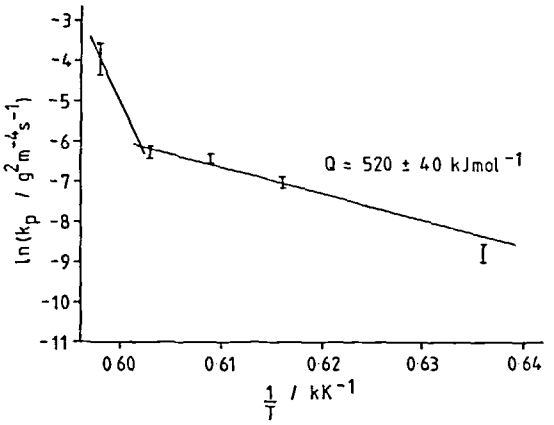

Fig. 13. Arrhenius treatment of oxidation mass gain data.

initially approximately parabolic, but at longer times (>200 ks) significant mass losses occurred (Fig. 12). This was assumed to be due to spalling of the oxide film during cooling to room temperature before weighing. For this reason the 1400°C point shown on the Arrhenius plot (Fig. 13), and based on an estimate of the initial rate constant, has been treated as approximate only.

Detailed microstructural and EPMA examination of these oxide films showed the oxide product at shorter times (<100 ks) to be a glass containing well-developed crystals of cristobalite (Fig. 14). Large voids were present at the glass–nitride interface. The composition of the glass was determined from multiple EPMA measurements to be MgO 34 mole%, SiO_2 58 mole% and Y_2O_3 8 mole%, together with trace amounts of impurity metals. This composition was in good agreement with that expected on the basis of the phase equilibrium diagram to be in equilibrium with SiO_2 at temperatures above the $MgSiO_3$–SiO_2–$Y_2Si_2O_7$ ternary eutectic (Fig. 2). At longer oxidation times considerable bloating of the oxide glass film occurred, which

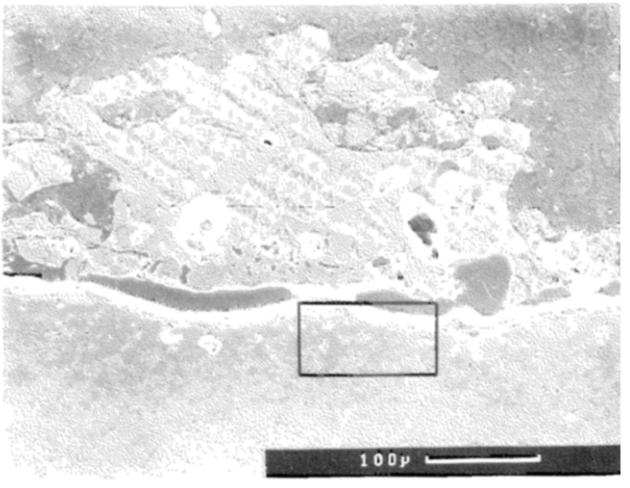

Fig. 14. Silicon nitride oxidised at 1400°C for ~85 ks. The oxide film consists of cristobalite crystals in a glass matrix. Indicated area is shown in Fig. 16.

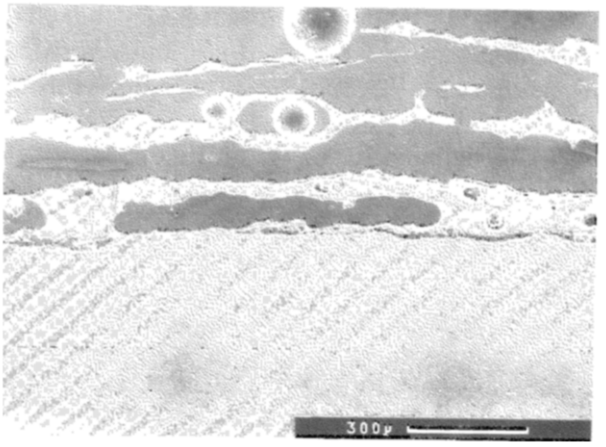

Fig. 15. Silicon nitride oxidised at 1400°C for ~172 ks, showing exfoliation of oxide film, containing silicon dioxide needles.

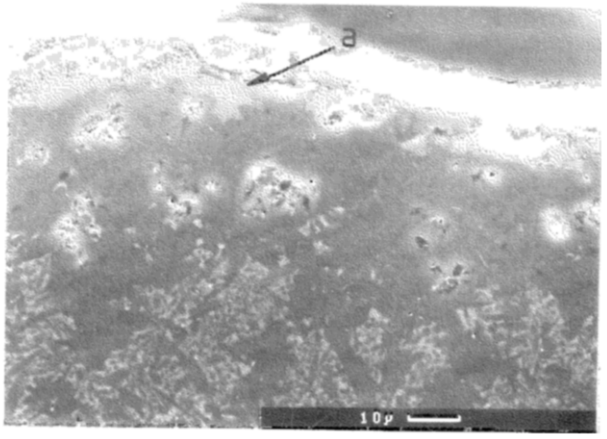

Fig. 16. Sample oxidised at 1400°C for ~85 ks. Secondary electron image of interfacial region indicated in Fig. 14. The silicon dioxide-rich layer at the silicon nitride surface is a magnesium–yttrium–silicate glass (a).

in section had developed a cellular, foamed appearance (Fig. 15).

The very thin film of glass at the nitride–oxide interface in samples oxidised for <250 ks (Fig. 16) had the approximate composition MgO 26 mole%, SiO_2 66 mole% and Y_2O_3 8 mole%, as determined by EPMA. It was therefore slightly rich in SiO_2, compared with the theoretical equilibrium composition, and with the mean composition of the glass nearer the silicate–air interface.

4 Discussion

4.1 Phase equilibrium relationships

The $MgO–SiO_2–Y_2O_3$ ternary oxide system examined is believed to describe satisfactorily the silicon nitride oxidation products. The omission of Cr_2O_3 in order to simplify the system is justified by the very low levels (<0·1 mass%) of Cr detected by EPMA in the glass product, and the failure to detect by XRD crystalline chromium-containing phases. The sintered silicon nitride contains the equivalent of 2·0 mole% of Cr_2O_3. An estimate may be made of the proportion of intergranular phase present on the basis of the amounts of metal oxide used to form the sintered material, and the silicon dioxide derived from the surface oxide film on the silicon nitride powder particles, together with the oxygen of the chromium oxide used. If all the chromium initially added subsequently resides in the intergranular phase (as $CrSi_2$) it can be estimated to constitute 12·6 mole% of this phase. The oxidation product film would be expected to contain 0·8 mole% of Cr_2O_3. That a very much smaller proportion of Cr appears to find its way to the oxidation product is presumed to be the result of the high degree of mobility of Mg^{2+} and Y^{3+} in the intergranular phase, which permits their outwards movement from unoxidised material and apparent preferential concentration in the surface oxide layer. The chromium only enters the oxide film as the $CrSi_2$ inclusions become absorbed by the advancing oxidation front.

The phase relationships observed at 1300°C and 1400°C are consistent with the broader qualitative picture of the $MgO–SiO_2–Y_2O_3$ system presented by Hampshire *et al.*[14] The ternary eutectic at ~1385°C lies very close to the $MgSiO_3–Y_2Si_2O_7$ join. From the calculated value of the MgO/Y_2O_3 molar ratio in the intergranular phase it can be seen that, in the absence of preferential diffusion, the oxidation products should have compositions on a line lying just to the $Y_2Si_2O_7$-rich side of the eutectic composition. Oxidation of the silicon nitride at temperatures below 1385°C should thus lead to the formation of proto-enstatite, cristobalite and yttrium disilicate, as is observed. At 1400°C the oxidation product should be cristobalite and yttrium disilicate, together with a large proportion (~90%) of liquid. In fact, oxidation yielded only cristobalite and liquid, indicating that preferential transfer of intergranular phase magnesium to the oxide film occurs.

The phase relationships established for the oxidation product system cannot be applied to the intergranular phase of the unoxidised silicon nitride. The intergranular phase appears, apart from the $CrSi_2$ inclusions, to be largely a glass, on the basis of the failure to detect by XRD significant amounts of crystalline phases other than β-Si_3N_4.

4.2 Oxidation behaviour

4.2.1 General observations

At the lower temperatures studied reasonable consistent parabolic kinetics were observed over

times of up to 450 ks. At the higher temperatures of 1385°C and 1400°C the kinetics appeared to be parabolic initially (at 1385°C to 250 ks, at 1400°C to 100 ks) but then became uncertain, with eventually loss of mass being seen. This loss seems likely to be due to cracking and spalling of the bloated oxide films on cooling, as a result of stresses arising from a combination of thermal expansion mismatch, the $\beta \rightarrow \alpha$-cristobalite transformation and external air pressure on the thin glass films. Fragments of glass were recovered from the sample holder.

Arrhenius treatment of the initial parabolic rate constants (estimated value for oxidation at 1400°C) showed two regions: below 1385°C a good fit of data was obtained, giving an experimental enthalpy of oxidation of $\sim 520\,\mathrm{kJ\,mol^{-1}}$; above 1385°C the reaction rate increased markedly, and no precise value for ΔH could be assigned. These two regions corresponding, within probable uncertainties of temperature measurement, to below and above the eutectic temperature, were associated with markedly different oxidation product microstructures, and are treated separately.

4.2.2 Low temperature oxidation

The typical distribution of products in the oxide film is shown schematically in Fig. 17. Because the basic oxidation reaction

$$Si_3N_{4(s)} + 3O_{2(g)} \rightarrow 3SiO_{2(s)} + 2N_{2(g)} \qquad (3)$$

yields nitrogen gas, the oxide film might be expected to show some evidence of this. At temperatures below the $MgSiO_3$–SiO_2–$Y_2Si_2O_7$ ternary eutectic of ~1385°C only crystalline phases are expected, and there is no liquid phase to make more clear the generation of a gas by, for example, bubble formation or bloating (as is certainly the case at higher temperatures). Within the silicate–cristobalite product phase, the presence of small voids at the silicon nitride–oxide interface must be taken as evidence for the location of reaction (3) at the nitride–oxide interface, as is generally assumed to be the case. The mechanism of nitrogen gas transport within the oxide film has never been satisfactorily established. In the present case we make the assumption that movement of molecular nitrogen, and its ultimate escape, by permeation through fissures and voids is the most likely mechanism.

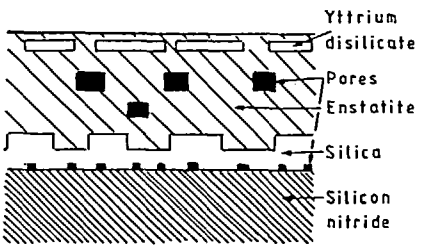

Fig. 17. Schematic diagram of product phase distribution in oxide film.

A more detailed examination of the kinetics of formation of the individual product phases, proto-enstatite, cristobalite and yttrium disilicate, shows significant differences. A striking feature, clear from SEM, EPMA and XRD examinations, is the relatively small amount of cristobalite present. This shows that an important component of the oxidation process is the reaction between the primary oxidation product silicon dioxide and magnesium oxide and yttrium oxide supplied from the intergranular phase, to form the two silicates which make up the major part of the overall oxidation product. The silicate formation reactions necessitate a continuous supply of metal cations and counter-balancing anions from the intergranular silicate. This is also an accepted feature of the oxidation mechanism for multiphase silicon nitride materials.[8] Examinations of the unoxidised silicon nitride adjacent to the oxide film have in previous studies demonstrated clearly the existence of a cation depletion zone, which can extend in the case of magnesium-containing intergranular phases for some considerable depth into the unoxidised material. In the present programme a detailed study of the unoxidised substrate microstructure was not made, but the EPMA traces indicated the necessary loss of Mg^{2+} extending over several tens of microns into the substrate. Yttrium depletion was harder to detect, which provided qualitative support to XRD analyses indicating preferential diffusion of Mg^{2+} to the surface oxide.

Formation of the proto-enstatite and yttrium disilicate followed approximately parabolic kinetics over times of up to 300 ks. An assessment of the relative rates of formation of these two phases on the basis of their XRD peak heights, and the calibration factors obtained from the analyses of artificial mixtures (Fig. 9), suggests that the rate of formation of proto-enstatite is approximately five times that of the yttrium disilicate. From the known composition of the intergranular phase, and an assumption of equal diffusion rates for Mg^{2+} and Y^{3+}, a ratio of proto-enstatite to yttrium disilicate of ~2·6 would be expected. Mg^{2+} mobility at these temperatures is thus greater than that of Y^{3+} by a factor of ~2 (greater Mg^{2+} mobility is also indicated by the phases produced on oxidation at 1400°C).

A notable feature of the structure of oxide films produced at these temperatures is that the proto-enstatite and yttrium disilicate phases are separated

from the silicon nitride (and cation source) by an apparently continuous layer of cristobalite. Moreover, much of the yttrium disilicate is separated from the silicon nitride, also by a thick band of proto-enstatite. It is thus clear that cation, and counterbalancing oxide ion, diffusion through cristobalite and, in the case of Y^{3+}, through enstatite, must occur readily under oxidation conditions. The tendency for yttrium disilicate to be located near to the silicate–air interface suggests further that yttrium disilicate nucleates first at the initial oxidising silicon nitride surfaces, and that these nuclei subsequently serve as the primary growth points for yttrium disilicate, to be moved further from the silicon nitride with development of the underlying cristobalite and enstatite layers.

The rate of formation of cristobalite is very much slower than the rates of the two silicates, and initially also follows parabolic kinetics. After ~150 ks the amount of cristobalite present appears to become constant. This could be a real effect, but it is more likely to be a consequence of the inaccuracy of the empirical XRD peak height correction method when applied to a layer of material at some distance below the surface of the oxide film. SEM photographs show the cristobalite layer to have a thickness of ~10 μm after 85 ks at 1370°C, with a total oxide film thickness of ~35 μm.

The reason for the abrupt change in the product ratio of proto-enstatite to yttrium disilicate at ~1350°C is not clear. It would be explicable in broad terms as the effect of a higher enthalpy of activation for the diffusion of Y^{3+} compared with that for Mg^{2+}, but the detailed reason remains to be established.

The high enthalpies of activation for the formation of both proto-enstatite and yttrium disilicate compared to the enthalpy of activation for mass gain are balanced by the lower enthalpy for cristobalite, and reflect a markedly more rapid silicate formation reaction at higher temperatures. All these values are too high to correspond to a single kinetic process, and are certainly composites derived from the temperature sensitivities of several linked mechanistic steps.

4.2.3 An oxidation model

Reaction of the primary oxidation product, silicon dioxide, with metal oxides released from the intergranular phase to form silicates has long been recognised as an essential feature of the oxidation of multiphase silicon nitride materials. A common assumption has been that the rate of oxidation is controlled by the outwards diffusion of intergranular phase cations[3] but the link between diffusion and oxidation has not been explicitly defined. Because cristobalite (in common with other forms of pure silicon dioxide) is an effective barrier to oxygen permeation,[15] its presence on the surface of silicon nitride must be assumed to be a primary factor controlling the oxidation rate of the silicon nitride. Any process influencing the thickness of this layer must also influence the oxidation rate, and one such process is, with the present multiphase material, reaction to form enstatite (and to a lesser extent yttrium disilicate).

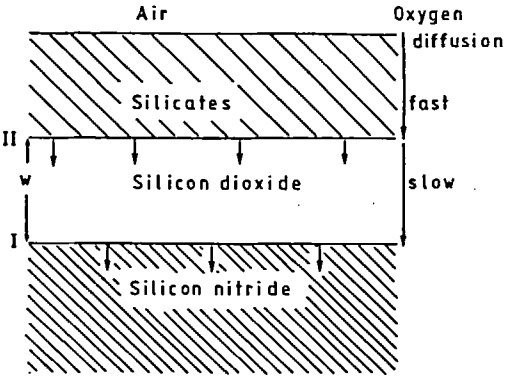

Fig. 18. Schematic of the material transport processes, and reactions taking place, in the Si_3N_4–$MgSiO_3$ interface region.

The continued oxidation/reaction process, in which cristobalite is simultaneously formed by oxidation of the silicon nitride and removed by reaction to form (primarily) enstatite, can be modelled as shown in Fig. 18. At interface I a silicon nitride grain is oxidised to cristobalite (with ~80% volume expansion). This process is assumed to be controlled by the slow rate of diffusion of oxygen through the cristobalite, and thus to follow parabolic kinetics. At interface II reaction of cristobalite to silicate occurs, at a rate controlled by the rate of supply of 'MgO' and 'Y_2O_3' from the intergranular phase. This reaction process is also assumed to follow parabolic kinetics, since it is controlled by the diffusion of ionic species down a cation chemical potential gradient between the glass (very approximately, and ignoring nitrogen, equivalent to '$Mg_2SiO_4.Y_2O_3$') and the cristobalite. Both processes may be described, and summed, mathematically as

$$\text{I oxidation} \qquad dw/dt = \alpha/w \tag{4}$$

$$\text{II silicate formation} \qquad dw/dt = -\beta t^{-1/2} \tag{5}$$

where w is the instantaneous cristobalite film mean thickness and α and β are reaction rate constants. Thus, combining eqns (4) and (5),

$$\frac{dw}{dt} = \frac{\alpha}{w} - \beta t^{-1/2} \tag{6}$$

An exact solution for eqn (6) is

$$w = kt^{1/2} \tag{7}$$

where

$$k = (\beta^2 + 2\alpha)^{1/2} - \beta \tag{8}$$

The oxidation rate equation is now

$$\frac{dP}{dt} = \frac{\alpha}{(\beta^2 + 2\alpha)^{1/2} - \beta} t^{-1/2} \tag{9}$$

whence

$$P = \frac{2\alpha}{(\beta^2 + 2\alpha)^{1/2} - \beta} t^{1/2} \tag{10}$$

where P is proportional to the distance advanced by the oxide interface into the silicon nitride, and hence to the recorded oxidation mass gain. P is necessarily a parabolic function of time, as indicated, because eqn (6) represents the difference between two parabolic functions.

Although oxygen permeation through cristobalite is slow, relatively fast oxidation of the multiphase silicon nitride can be seen because the protective cristobalite layer is maintained at a thinner level than would otherwise be the case, by the supply of silicon nitride intergranular phase cation and reaction to form silicate. This model rests, of course, on the assumption that inwards oxygen diffusion through a continuous (primarily proto-enstatite) layer is relatively fast and thus not rate-controlling. SEM observations of the silicate layer show a significant density of fissures and voids, and it is unlikely to be an effective barrier to the gaseous transport of oxygen.

While the model is mathematically satisfactory and eqn (10) provides the required causal link between observed oxidation rate and grain-boundary cation diffusion processes leading to the formation of a silicate rather than cristobalite as the major oxidation product, for it to be completely satisfactory values for the two rate constants must be obtained and shown to be related to accepted values of permeation or diffusion coefficients.

Values for β can readily be obtained directly from XRD analyses of the oxide film, and the measure of the total silicon dioxide content (as cristobalite and silicate) of the film, obtained from oxidation mass gain measurements. Values for α are derived from eqn (10), again on the basis of the oxidative mass gains and the calculated values for P. Table 4 shows these data for three temperatures. β^2 is also shown because this term is the effective rate constant for silicate formation and thus contains the diffusion coefficient. It is difficult to make immediate use of the β^2 term because values of diffusion coefficients for Mg^{2+} and Y^{3+} in silicate glasses of the type formed here have not been reported.

Table 4. α and β values calculated for silicon nitride oxidation

θ (°C)	α ($10^{-16} m^2 s^{-1}$)	β ($10^{-8} m s^{-1/2}$)	β^2 ($10^{-16} m^2 s^{-1}$)
1 300	0·53	0·70	0·49
1 350	2·9	2·5	6·5
1 385	5·2	4·4	20

The α term is believed to represent the permeation coefficient for oxygen through cristobalite, values which also have not been reported previously. For vitreous silica at 1100°C the permeation coefficient is 10^{-12} m^2 s^{-1}.[16] Oxygen diffusion in crystalline silica is several orders of magnitude slower than in vitreous silica,[17] and a similar difference for permeation might be expected.

4.2.4 High temperature oxidation

At 1385°C the oxidation product still consists of the three crystalline phases, although the phase equilibrium diagram indicates that at least one of the three should be unstable. The discrepancy between the observations at 1385°C, on the hot-stage microscope and after oxidation, is likely to be due to slight temperature measurement errors between the two experimental systems. At 1400°C the product is cristobalite and a low viscosity liquid. Enrichment of the oxide film with magnesium relative to yttrium is clearly occurring because the expected product is yttrium disilicate, cristobalite and liquid.

SEM examination of films formed at 1400°C shows large differences compared with the films developed at 1385°C and lower temperatures. It is clear that much of the product has been a mobile liquid, and extensive bloating and exfoliation has occurred. That parabolic kinetics are still observed in at least the initial stages of reaction clearly cannot be explained in terms of oxygen diffusion through a silicate layer of steadily increasing thickness. The model described in Section 4.2.3 is still applicable, however, since the process occurring at interface II, the solution of cristobalite in a liquid silicate slightly enriched with MgO and Y_2O_3 relative to the composition on the SiO_2–liquidus surface at 1400°C, replaces the solid-state reaction to form enstatite.

Observations of the formation at 1400°C of a glass layer at the nitride–silicate interface richer in SiO_2 than predicted would be explicable in terms of the dissolution of cristobalite into an apparently slightly supersaturated liquid silicate. This suggests that at higher temperatures the rate of solution of

cristobalite is becoming an additional factor in the overall rate-controlling process.

The discontinuity in the oxidation rate constant seen at 1400°C seems most likely to be associated with the change in nature of the oxide film at the eutectic temperature. It is unlikely to be due to events within the silicon nitride intergranular phase, which is a glass and therefore will show only smooth changes in behaviour with change of temperature. A possible explanation lies in the observed morphology of the product cristobalite above the eutectic temperature. This shows a spiky morphology, with individual crystallites growing unhindered into the liquid silicate, rather than the more uniformly thick 'fish scale'[18] type of cristobalite film formed at the enstatite interface at sub-eutectic temperatures. The cristobalite may not adequately protect the underlying bulk silicon nitride. Extensive internal oxidation of the nitride at the nitride–oxide interface will thus start to occur with oxygen penetration into the intergranular glass. The overall effect is that at the eutectic temperature there is a sudden, marked increase in the reactant interface area. The reaction of individual silicon nitride grains will now be generally in accord with the model described above, and giving continuing parabolic kinetics, rather than the silicon nitride continuum. Close examination of the silicon nitride at the oxide interface shows microstructural changes which are consistent with internal oxidation at depths up to 50 μm below the surface (Fig. 14).

The results of this investigation of a silicon nitride sintered with MgO and Y_2O_3 additions are broadly in line with those reported by Babini *et al.*[12] for the oxidation of a less pure, hot-pressed, silicon nitride containing 8 mass% Y_2O_3 (5·0 mol%) and 1 mass% MgO (3·5 mole%), a Y_2O_3/MgO molar ratio of 1·4. A similar change in activation enthalpy from 580 kJ mol^{-1} to a much higher value occurred at ~1350°C. This would be consistent with a lower eutectic temperature for an oxide film containing significant amounts of calcium and aluminium. At about this temperature also, marked changes in the oxide film were observed, with, as would be expected, decreases in the amount of enstatite and yttrium disilicate. At ~1300°C the enstatite/yttrium disilicate ratio was ~3. It is thus clear that in both the hot-pressed and the present sintered material, the lesser amount of intergranular phase Mg^{2+} has a significant degree of control over the oxidation process. The change in oxidation behaviour at 1350°C was attributed in the earlier work to a softening of the intergranular phase. This phase was a glass and was unlikely to undergo an abrupt change at a specific temperature. The reason for the change in oxidation behaviour must therefore be related to the changed composition and morphology of the oxidation products above the eutectic temperature.

To achieve the maximum resistance to oxidation in a multiphase silicon nitride, the materials' related requirements thus appear to be:

(1) a minimum quantity of intergranular phase;
(2) cations of low mobility in this phase;
(3) a high eutectic temperature for the oxidation product–silicon dioxide system.

The last point indicates the need for a chemically pure and compositionally simple intergranular phase system in order to minimise the number of components contributing to the eutectic composition.

5 Conclusions

The oxidation behaviour of the MgO- and Y_2O_3-containing sintered silicon nitride can be related to the phase equilibrium relationships describing the oxidation products. Phases observed in the oxide film are those expected on the basis of the $MgSiO_3$–SiO_2–$Y_2Si_2O_7$ compatibility triangle, for which the ternary eutectic temperature is ~1385°C. Mg^{2+} is approximately twice as mobile as Y^{3+} in the silicon nitride intergranular glass, and to a considerable extent therefore the behaviour of this silicon nitride is controlled by the presence of the magnesium.

A thin cristobalite film at the silicon nitride–silicate interface provides a barrier to oxygen diffusion and is the second of the two rate-controlling factors. It is believed that the morphological differences seen in the cristobalite, below and above the oxide product eutectic temperature, are responsible for the markedly faster oxidation rate seen above ~1385°C. At the higher temperatures liquid development permits the replacement of a continuous cristobalite film by localised crystal growth. Enhanced rates of oxidation of individual silicon nitride grains at the nitride–oxide interface effectively increase the reaction interface area.

Values have been tentatively assigned to the permeation coefficients for oxygen in cristobalite at temperatures between 1300°C and 1385°C.

Acknowledgements

This work was supported by an SERC CASE Studentship. Rolls Royce plc is thanked for as-

sistance with the supply of materials, and with electron microprobe analyses.

References

1. Drew, R. A. L., Hampshire, S. & Jack, K. H., Nitrogen glasses. In *Special Ceramics 7*, ed. D. Taylor & P. Popper. *Proc. Brit. Ceram. Soc.*, **31** (1981). The British Ceramic Society, Stoke-on-Trent, UK, pp. 119–32.
2. Singhal, S. C., Oxidation of silicon nitride and related materials. In *Nitrogen Ceramics*, ed. F. L. Riley. Noordhoff, Leiden, The Netherlands, 1977, pp. 607–26.
3. Singhal, S. C., Thermodynamics and kinetics of oxidation of hot pressed silicon nitride. *J. Mater. Sci.*, **11** (1976) 500–9.
4. Cubicciotti, D. & Lau, K. H., Kinetics of oxidation of hot pressed silicon nitride containing magnesia. *J. Am. Ceram. Soc.*, **61**(11–12) (1978) 512–17.
5. Chukukere, F. N. & Riley, F. L., Mass transport processes in the oxidation of calcium doped β'-sialon. In *Mat. Sci. Forum*, Vol. 7, 1986, ed. R. Freer & P. F. Dennis. Trans. Tech. Publications, Switzerland, pp. 307–16.
6. Mieskowski, D. M. & Sanders, W. A., Oxidation of silicon nitride densified with rare-earth oxides. *J. Am. Ceram. Soc.*, **68**(7) (1985) C160–C163.
7. Kiehle, A. J., Heung, L. K., Gielisse, P. J. & Rockett, T. J., Oxidation behaviour of hot-pressed silicon nitride. *J. Am. Ceram. Soc.*, **58**(1–2) (1975) 17–20.
8. Clarke, D. R. & Lange, F. F., Oxidation of silicon nitride alloys: relation to phase equilibrium in the system Si_3N_4–SiO_2–MgO. *J. Am. Ceram. Soc.*, **63**(9–10) (1980) 586–93.
9. Singhal, S. C., Oxidation and corrosion–erosion behaviour of silicon nitride and silicon carbide. In *Ceramics for High Performance Applications—2*, Army materials conference series, ed. J. J. Burke, A. E. Gornum & R. N. Katz. Brook Hill Publishing, Chestnut Hill, MA, 1974, pp. 533–48.
10. Cubicciotti, D. & Lau, K. H., Kinetics of oxidation of yttria hot pressed silicon nitride. *J. Electrochem. Soc.*, **126**(10) (1979) 1723–8.
11. Babini, G., Bellosi, A. & Vincenzini, P., Oxidation of silicon nitride hot-pressed with ceria. *J. Am. Ceram. Soc.*, **64**(10) (1981) 578–84.
12. Babini, G. N., Bellosi, A. & Vincenzini, P., Oxidation of silicon nitride hot-pressed with Y_2O_3 + MgO. *J. Mater. Sci.*, **18** (1983) 231–44.
13. Cotton, J. W. & Swindells, R. European patent application 0 107 919, 9 May 1984.
14. Hampshire, S., Pomeroy, M. J. & Saruhan, B., Kinetics of sintering of silicon nitride with mixed oxide additives. In *High Tech Ceramics*, ed. P. Vincenzini. Elsevier, Amsterdam, 1987, pp. 941–51.
15. Bremen, W., Naoumidis, A. & Nickel, H., Oxidationsverhalten des Pyrolytisch abgeschiedenen—SiC unter einer atmosphare aus CO-CO_2 gasgemischen. *J. Nucl. Mater.*, **71** (1977) 56–64.
16. Norton, F. J., Permeation of gaseous oxygen through vitreous silica. *Nature*, **191** (1961) 701.
17. Schachtner, R. & Sockel, H. G., Study of oxygen diffusion in quartz by activation analysis. In *Proc. Int. Symp. on the Reactivity of Solids*, ed. J. Wood, O. Lindquist & C. Helgesson. Plenum, New York, 1976, pp. 605–9.
18. Roberts, E. W., Petrology and density of flint: Pt I. Flint calcined at 1400°C. Research Paper No. 254, *Research Papers of the British Ceramic Research Association*, Vol. VII, 1954.